Restraint mechanisms in precast concrete double-tee floor systems subjected to fire

Nader M. Okasha and Stephen Pessiki

- This paper examines restraint mechanisms in precast, prestressed concrete double-tee beams typically used in structures exposed to fire.
- The study examines idealized (simple and fixed) single-span restraints and three realistic restraint mechanisms: multiple successive spans, gravity support elements (for example, spandrels or inverted-tee girders), and flange connectors.

The structural behavior of a precast, prestressed concrete floor system subjected to fire is influenced by the end restraint condition of its elements. Current design practice in the United States uses a dual classification for fire resistance of supporting members in floor and roof systems in buildings, depending on whether these members are restrained or unrestrained at their ends. There are significant differences between restrained and unrestrained conditions in terms of the suitability of a given section for a given span and loading condition.

Chapter 6 of *Design for Fire Resistance of Precast Prestressed Concrete*[1] suggests that restraint comes primarily from end supports. In actual precast concrete structures, restraint may come from a variety of effects in addition to the conditions that exist at the end supports of a member. For example, restraint may be provided by connections between adjacent members not subjected to fire.

The objective of this paper is to analytically investigate the development of restraint mechanisms in precast, prestressed concrete structures under fire loading. A prototype precast, prestressed double-tee beam typically used in practice is considered. The importance of various restraint mechanisms was investigated by evaluating their influence on the strength of the double-tee beam section.

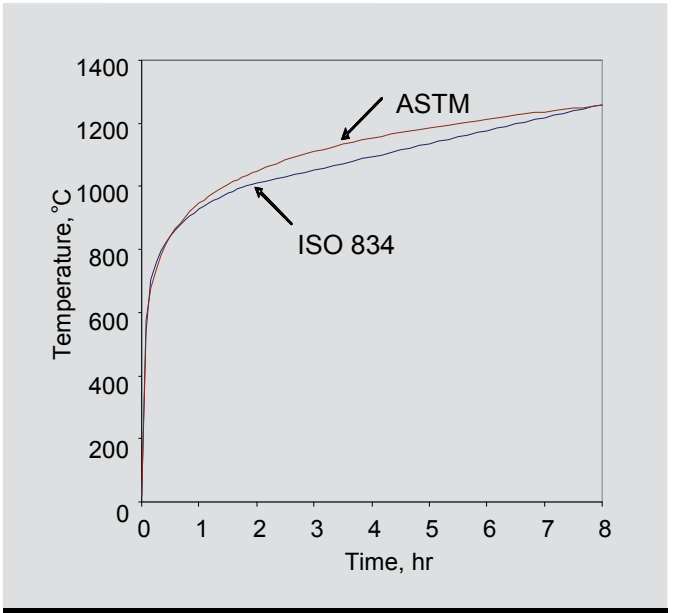

Figure 1. Standard fire time-temperature curves. Note: °C = (°F – 32)/1.8.

The study examined the two idealized (simple and fixed) single-span restraint conditions, as well as three realistic restraint mechanisms: multiple successive spans, gravity support element restraints (for example, spandrels or inverted-tee girders), and flange connectors. Okasha[2] and Okasha and Pessiki[3] give complete details of the study represented in this paper.

Methodology

The analytical approach consisted of three sequential steps:

1. Nonlinear heat transfer analysis.
2. Nonlinear structural analysis.
3. Nonlinear strength analysis.

Each step uses the results from the previous step.

The nonlinear heat transfer analysis was performed to determine the magnitude of temperature throughout a double tee at different fire durations. The nonlinear structural analysis was performed to determine the magnitude and location of restraint forces developed in the double tee resulting from various restraint conditions prescribed at different fire durations. Finally, the nonlinear strength analysis was performed to determine the section strength of the double tee at the different fire durations considered.

Nonlinear heat transfer analysis

Nonlinear finite element transient heat transfer analyses were conducted to determine the distribution and magnitude of temperature throughout a double tee at different times during the standard fire. The analyses are nonlinear because material properties are temperature dependent.

The analyses are transient because the temperatures vary with time in fire tests and an overall temperature history needs to be solved for the following structural analysis step. The double-tee model was only exposed to fire from its underside.

The nonlinear heat transfer analyses in this paper were conducted using computer software. The element type used for the heat transfer analysis step was a solid (continuum) first order (eight nodes) hexahedron (brick) element, and it was used with a full integration solution technique.

In typical studies of fire resistance, it is common to expose structural elements to heating in accordance with a standard temperature-time relation. Standard time-temperature curves specify the furnace temperature as a function of time for a fire test. **Figure 1** presents the most widely used standard fire tests ASTM E119[4] and ISO 834-2.[5] In this paper, the ASTM E119 time-temperature curve is used.

Nonlinear structural analysis

Nonlinear structural analyses were conducted after the heat transfer analyses to determine the restraint forces developed in the models and resulting from various restraint conditions prescribed at different fire durations (for example, 0.5, 1.0, 1.5, and 2.0 hours). The structural analyses were also conducted using the computer software.

The computer software provides an option of running the structural analysis either coupled with or uncoupled from the heat transfer analysis. In this paper, sequential uncoupled analyses were performed. This option considers that the structural analysis results have no bearing on the heat transfer analysis (for example, the thermal properties are not dependent on stress).

The element type used for the structural analysis step was a solid (continuum) first order (eight nodes) hexahedron (brick) element enhanced with incompatible modes and used with a full integration technique. The element type and mesh configuration must be consistent with those used in the preceding finite element transient heat transfer analysis because the nodal temperature output of the heat transfer step is an input applied to the same nodes in the structural analysis step.

Nonlinear strength analysis

The results from the previous analyses were used to determine the section strength at the fire durations considered and for the restraint forces developed under the various boundary conditions. This was done using nonlinear fiber analysis with different computer software. A different fiber model was built for each fire duration, with the material properties adjusted for temperature effects. The loads are applied to the model in the following sequence:

1. The prestressing forces resulting from the prestressing steel.

2. The restraint forces resulting from the previous structural analysis step.

3. Increasing curvature to failure of the section.

The outcome of these analyses is the strength of the double-tee beam subjected to different restraint conditions at different fire durations. This provides the insight needed to understand the effect of fire on precast concrete members subject to different restraint conditions.

Modeling of material properties

Concrete

Normalweight concrete with siliceous aggregates was used. The material properties that affect the heat transfer analysis are thermal conductivity and specific heat.

Thermal conductivity is the property of a material that indicates its ability to conduct heat. The thermal conductivity of concrete tends to decrease with the rise in temperature for normalweight concrete. The thermal conductivity of concrete is found using Eq. (1) and (2).[6]

$$k = -0.000625T + 1.5 \quad \text{for} \quad 0°C \le T \le 800°C\ (1472°F) \tag{1}$$

$$k = 1.0 \text{ for } T > 800°C \tag{2}$$

where

k = thermal conductivity (W/m°C)

T = temperature (°C)

Specific heat of a material is the amount of energy required to raise the temperature of one gram of that material by one degree Celsius. Equations (3) through (7)[6] give the relation between the volumetric specific heat (product of specific heat and density) and temperature for concrete with siliceous aggregates.

$$\rho_c C = (0.005T + 1.7) \times 10^6 \text{ for } 0 \le T \le 200°C\ (392°F) \tag{3}$$

$$\rho_c C = 2.7 \times 10^6 \text{ for } 200 < T \le 400°C\ (752°F) \tag{4}$$

$$\rho_c C = (0.013T - 2.5) \times 10^6 \quad \text{for} \quad 400 < T \le 500°C\ (932°F) \tag{5}$$

$$\rho_c C = (-0.013T + 10.5) \times 10^6 \text{ for } 500 < T \le 600°C\ (1112°F) \tag{6}$$

$$\rho_c C = 2.7 \times 10^6 \text{ for } T > 600°C \tag{7}$$

where

ρ_c = density of concrete (24,000 N/m^3)

C = specific heat (J/m^3°C)

The constitutive relations of concrete are also temperature dependent. Equations (8) through (12) provide a family of stress-strain relations for siliceous aggregate concrete.[6]

$$\varepsilon_{max} = 0.0025 + (6.0T + 0.04T^2) \times 10^{-6} \tag{8}$$

$$f_c' = f_{co}' \text{ for T} < 450°C\ (842°F) \tag{9}$$

$$f_c' = f_{co}' \left[2.011 - 2.353 \left(\frac{T - 20}{1000} \right) \right] \text{ for } T \ge 450°C \tag{10}$$

$$f_c = f_c' \left[1 - \left(\frac{\varepsilon_{max} - \varepsilon_c}{\varepsilon_{max}} \right)^2 \right] \quad \varepsilon_c \le \varepsilon_{max} \tag{11}$$

$$f_c = f_c' \left[1 - \left(\frac{\varepsilon_c - \varepsilon_{max}}{3\varepsilon_{max}} \right)^2 \right] \quad \varepsilon_c > \varepsilon_{max} \tag{12}$$

where

f_c = compressive strength of concrete at temperature T

f_c' = cylinder strength of concrete at temperature T

f_{co}' = cylinder strength of concrete at temperature 20°C (68°F)

ε_c = strain of the concrete

ε_{cmax} = strain corresponding to maximum stress

Figure 2 presents these relations for the 34.8 MPa (5050 psi) compressive strength siliceous aggregate concrete used in this paper. Each of the curves shown in the figure presents a constitutive model for this concrete at a given temperature.

The coefficient of thermal expansion of concrete α varies linearly with temperature (Eq. [13]).

$$\alpha = (0.008T + 6) \times 10^{-6} \tag{13}$$

Prestressing steel

The prestressing steel had an ultimate strength f_{pu} of

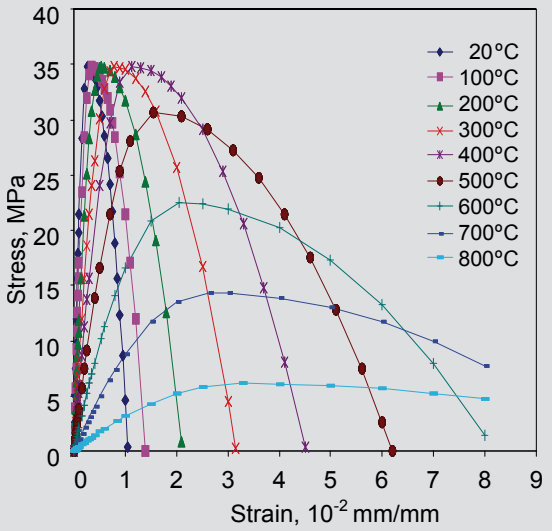

Figure 2. Temperature-dependent stress-strain curves for concrete. Source: Data from Lie (1992). Note: 1 mm = 0.394 in.; 1 MPa = 0.145 ksi; °C = (°F – 32)/1.8.

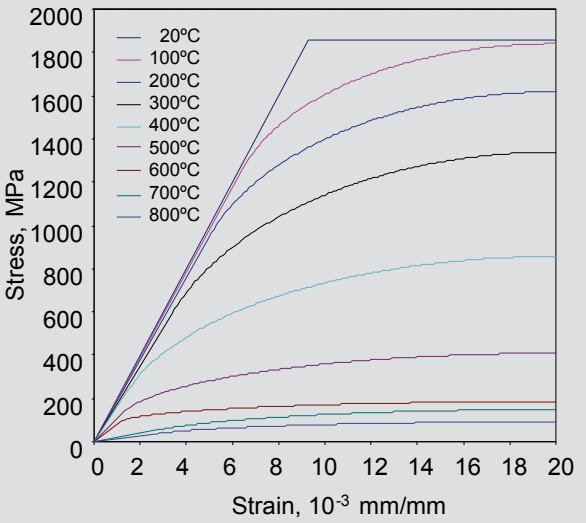

Figure 3. Stress-strain curves for prestressing steel. Source: Data from Thompson (2004). Note: 1 mm = 0.394 in.; 1 MPa = 0.145 ksi; °C = (°F – 32)/1.8.

1860 MPa (270 ksi) and an effective stress f_{pe} of 1221 MPa (177 ksi). Another family of stress-strain curves (**Fig. 3**) was derived for the prestressing steel at various elevated temperatures. These curves are computed according to equations provided by Eurocode 2 part 1.2.[7]

Because the computer software does not account for prestress in steel, a rational approach was adapted and successfully used by Thompson[8] to include the prestressing forces in the model. This approach was also adapted in this paper by both modifying the stress-strain diagram of the prestressing steel to model the initial stresses in the strands and applying an equivalent prestressing force to the model at the end nodes equal to the forces provided by the prestressing strands on the concrete beam.

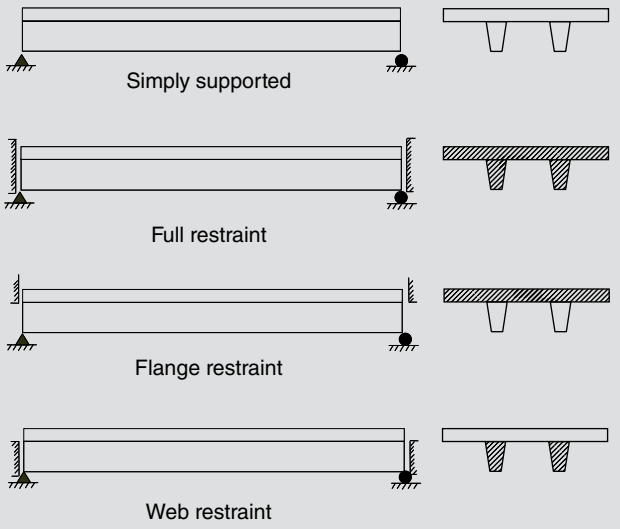

Figure 4. Boundary condition cases.

Idealized boundary condition analyses

In these analyses, a single-span double-tee beam was analyzed for four different idealized boundary conditions, and the strength of the double-tee beam at four different fire durations (0.5, 1.0, 1.5, and 2.0 hours) was examined. **Figure 4** shows the four idealized boundary condition cases. A simply supported beam was considered an unrestrained boundary condition. The restrained cases were the following:

- full restraint, where the entire section of the double-tee beam at the supports is restrained
- flange restraint, where only the flange of the double-tee beam at the supports is restrained
- web restraint, where only the web of the double-tee beam at the supports is restrained.

These boundary conditions are bounding cases in the sense that the restrained parts of the models are attached to an infinitely stiff element providing infinite compression restraint to these parts. In real structures, double-tee beams are attached to other members or systems of members possessing finite stiffness.

Heat transfer analysis

Figure 5 shows the cross section of the prototype double-tee beam. The prototype was a 15DT34 beam and strand pattern 188-S (18 strands with 13 mm [0.5 in.] diameter) beam provided by the *PCI Design Handbook: Precast and Prestressed Concrete*.[9] The beam had a span of 18.6 m

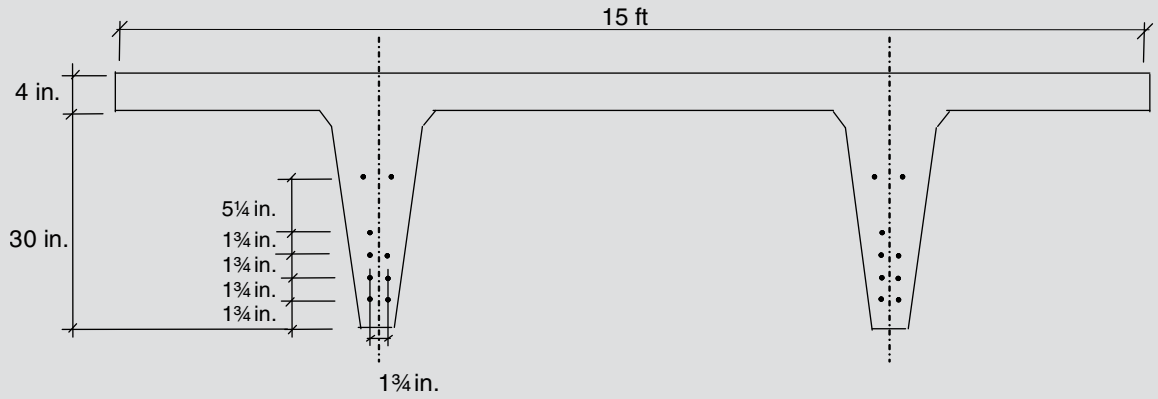

Figure 5. Cross section of the prototype double-tee beam (not to scale). Note: 1 in. = 25.4 mm; 1 ft = 0.305 m.

(61 ft), a flange depth of 100 mm (4 in.), flange width of 4.6 m (15 ft), web depth of 760 mm (30 in.), web upper width of 230 mm (9 in.), and lower width of 165 mm (6.5 in.). The prestressing strands are placed as shown in Fig. 5; they have an ultimate stress of 1860 MPa (270 ksi) and effective prestress of 1220 MPa (177 ksi).

The mesh configuration for the double-tee beam was selected based on heat transfer convergence studies and providing an appropriate number of nodes on the sides of the model to accommodate the various cases of mechanical boundary conditions prescribed in the structural analysis steps. Accordingly, **Fig. 6** shows the mesh selected for heat transfer and structural analysis. The mesh includes three elements through the flange thickness and four elements across the web width.

Next, a nonlinear heat transfer analysis was conducted for the model to obtain the nodal thermal histories at four different fire durations (0.5, 1.0, 1.5, and 2.0 hours). **Figure 7** shows the resulting temperature contours over the double-tee beam section at the end of each fire duration. The thermal histories were also used in the finite element structural analysis as thermal load. The temperature contours were used to build the fiber analysis model.

Temperatures of the prestressing steel were extracted from the results of these analyses by linear interpolation between the temperatures of the adjacent nodes. The prestressing steel strands were placed at five levels, and the strands of each level had the same temperature in both webs and at both sides of the centerline of the web because they were the same distance from the centerline. In reference to Fig. 5, level 1 is the closest to the bottom web. **Table 1** presents temperatures at these five levels for the four different fire durations. These temperatures were used later in the strength analysis to assign the appropriate mechanical properties for each strand.

Restraint forces analyses

Attention in this paper is focused on the effect of the axial thermal deformations of the structural elements on the strength of these elements. Therefore, mechanical boundary conditions were prescribed to provide restraint in the longitudinal direction only, and freedom of expansion was granted in the other directions by providing minimum global constraints to prevent instabilities and rigid body motions in the model and matrix singularity problems in the analysis.

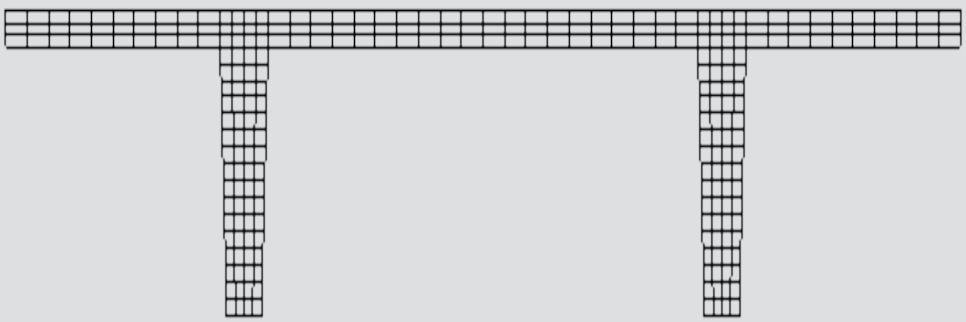

Figure 6. Mesh configurations of the double-tee beam.

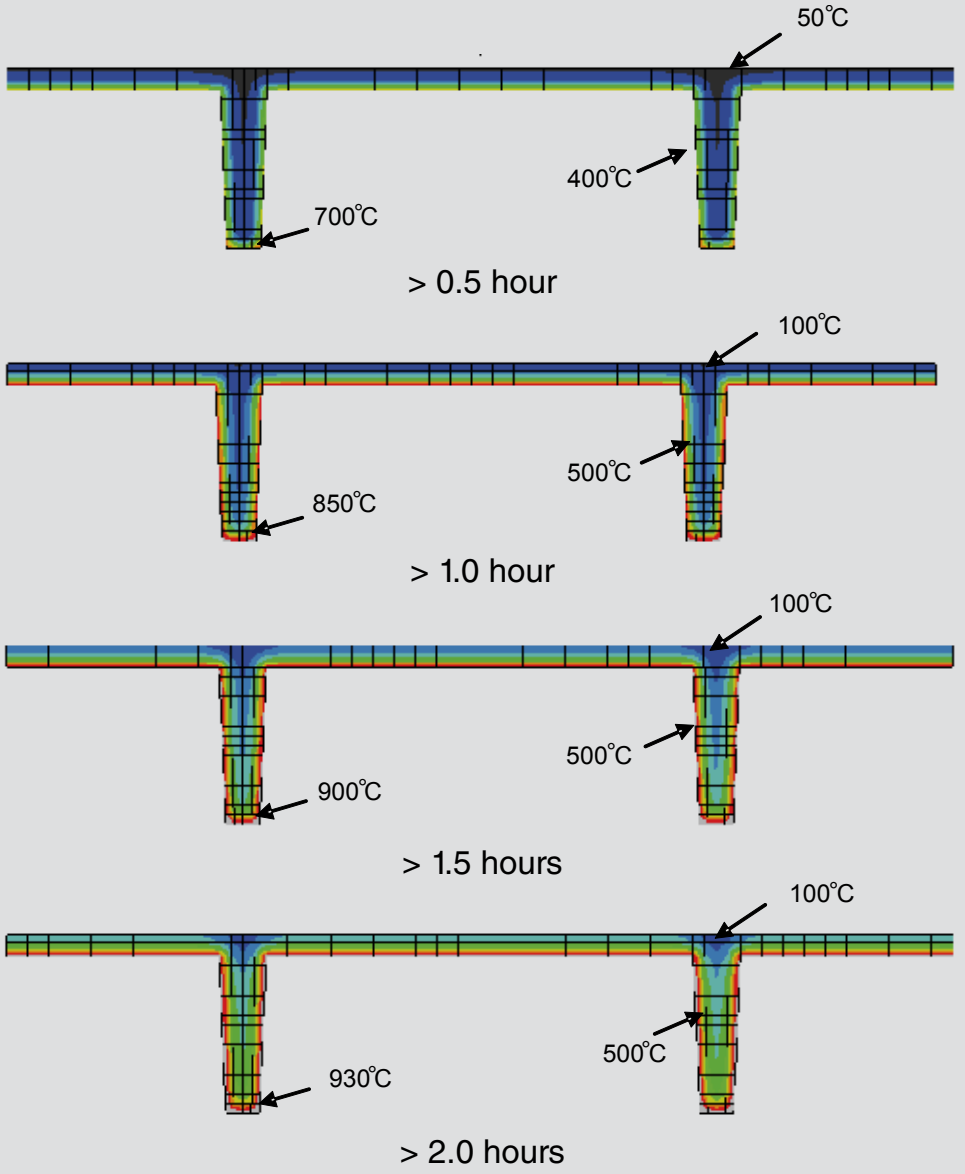

Figure 7. Temperature distribution contours over the cross section of the double-tee beam for different fire durations. Note: °C = (°F – 32)/1.8.

Table 1. Temperature at the levels of the prestressing steel strand levels

Level	Temperature at fire durations, °C			
	0.5 hour	1.0 hour	1.5 hour	2.0 hour
1	181	408	542	646
2	101	263	406	507
3	88	218	355	453
4	85	203	334	430
5	81	188	304	398

Note: °C = (°F – 32)/1.8.

Table 2. Restraint forces results for the ideal boundary conditions

Load effect	Axial force, kN*				Bending moment, kN-m†			
Fire duration, hours	0.5	1.0	1.5	2.0	0.5	1.0	1.5	2.0
Full restraint	8597	10,363	10,786	10,532	-294	-6	170	282
Flange restraint	6116	7815	8369	8365	712	963	1040	1042
Web restraint	7479	8897	9267	9073	-486	-265	-100	-21

* Positive values are in compression.

† Positive value moments cause compression above neutral axis.

Note: 1 m = 3.28 ft; 1 kN = 0.225 kip.

The longitudinal restraints prescribed were compression-only restraints. The nodes restrained were allowed to move away from the support and not toward the support, resulting only in compression forces at the support. This was done to capture the behavior of double-tee beams in real structures where the restraint due to thermal expansion results from the double-tee beam pushing against the structural components with which it is in contact. This compression-only property was provided to the support using nonlinear springs having infinite stiffness in compression and negligible stiffness in tension. These springs were connected between all the nodes located in the region restrained and the ground (an infinitely rigid object). The forces developed in these springs were the restraint forces sought.

Table 2 shows the axial restraint forces and moments found from the analyses. The direction of the restraint moment was consistent with the restraint condition. The flange-restraint case experienced positive restraint moments throughout the duration of the fire and the web-restraint case experienced negative restraint moments. The full-restraint case, however, experienced negative restraint moment during the early stages of the fire and then the moment reversed. The beam started behaving as being restrained from the web and then continued to behave as being restrained from the flange. This is attributed to the effect of the material softening due to the high temperatures toward the bottom of the beam causing the location of the resultant to move upward.

Strength analyses

The fiber analysis model used in this step comprised one fiber element that was fixed at one end and free at the other. The behavior of this element was monitored at the center, which is called the slice. The slice, and hence the element, comprised a number of fibers, which were defined by their areas, material properties, and distance from a selected datum. Axial loads were applied during the analysis at the datum. The datum chosen for the double-tee beam was the centroid of its original unheated cross section. Each fiber was assigned a stress-strain relationship with either concrete or steel material properties. The concrete fibers were built by discretizing the thermal distribution contours resulting from the previous finite element heat transfer analyses. These contours were specially assigned a uniform scale from 50°C to 850°C (122°F to 1562°F) with 100°C (180°F) intervals, so each color represented a range of temperatures with an average to be a multiple of 100°C. Thus, each color was assigned one of the stress-strain curves that are related to the temperatures in the multiples of 100°C. Therefore, the fibers were discretized so that each fiber was assigned the color that dominates its area, and hence the corresponding stress-strain relation. The highest temperature considered was 800°C (1472°F); any fibers with temperatures higher than that were still assigned the 800°C relations. Any fibers with temperatures below 50°C were assigned room temperature properties (20°C [68°F]).

The number of fibers in the models ranged from 200 to 250. The fineness of the discretization provided greater accuracy in the analysis results. **Figure 8** shows one half of the double-tee beam section with its discretized fibers after one hour of fire exposure as an example. Because of the symmetry of the cross section, only one half is shown. The steel fibers were assigned the properties corresponding to the temperatures closest to their temperatures that are found by interpolating between the nodal temperatures in the heat transfer analysis step.

Figure 9 provides a group of curves presenting the results of the fiber analysis. The strength of the double-tee beam varied significantly with the boundary conditions prescribed and subjected to a given duration of standard fire. The strength was significantly less in the flange-restraint case, and even less in the simply supported case, than in the web-restraint case and the full-restraint case. Figure 9 also shows that the strength of the double-tee beam in the web-restraint case was slightly higher than in the full-restraint case. This is attributed to the fact that the flange contributes to the restraint in the full-restraint case (which tends to decrease the strength) and does not in the web-restraint case. By comparing these results with

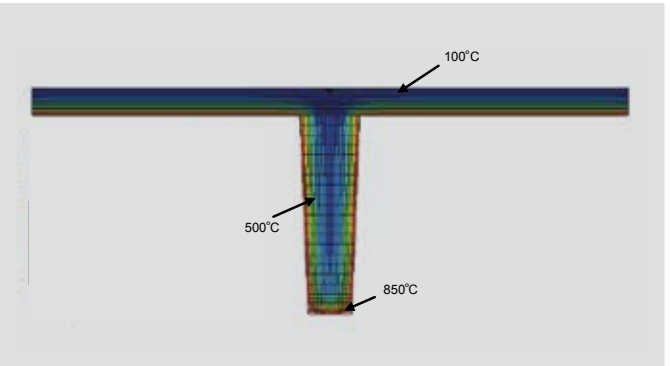

Figure 8. Cross section of one half of the double-tee beam with the analysis model fibers at fire duration of 1.0 hour. Note: °C = (°F – 32)/1.8.

the self-weight midspan moment of the simply supported double-tee beam (that is, 778 kN-m [6890 kip-in.]), the simply supported double-tee beam is expected to fail under its self-weight if exposed to two hours of fire.

Multiple-span restraints

These analyses were conducted to capture the behavior of a case of real restraint in precast concrete structures. Multiple-span restraint refers to the case in which double-tee beams are arranged in a floor system in series with other double-tee beams, and the restraint forces develop from their interaction. The restraint forces generated in the double tee depend on the stiffness of the beams connected to it and the type of connection. Two systems of double-tee beams were considered and are referred to as the three double-tee system and the five double-tee system (**Fig. 10**). In both systems, the middle double-tee beam has the same geometry, mesh, element type, and material properties that were discussed and used in the idealized cases. In addition, only the middle double-tee beam was exposed to the standard fire from below. The other double-tee beams remained at room temperature and retained their room-temperature properties to isolate their role in providing restraint. Thus, the same thermal histories generated in the previous analyses can be used in these analyses. Therefore, only the nonlinear finite element structural analyses were conducted and the thermal histories were used as a thermal load input. These analyses result in the restraint forces that were then used in subsequent fiber model analyses to find the strength of the double-tee beam for each case.

Restraint force analyses

To reduce analysis time, the room temperature double-tee beams were modeled by three-dimensional frame elements attached to a transition mesh at the supports (Fig. 10). In the three double-tee beam system, each room-temperature double-tee beam was made of one frame element attached to a transition mesh at each end. In the five double-tee beam system, two frame elements were directly connected to each other on each side of the middle, heated double-tee beam and attached to a transition mesh at each support end.

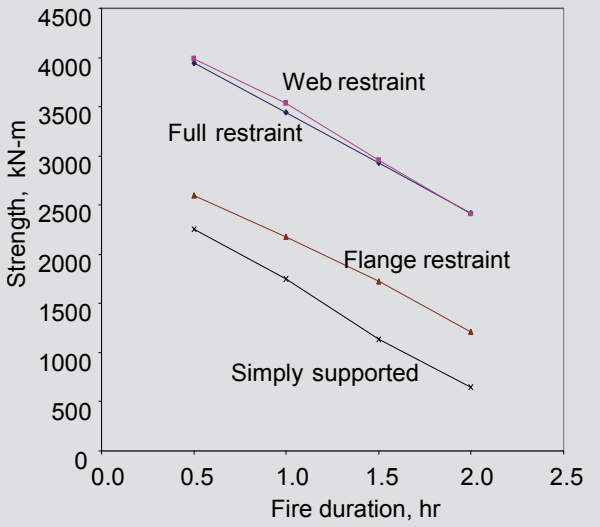

Figure 9. Summary of strength analyses for the idealized boundary condition cases. Note: 1 m = 3.28 ft; 1 kN = 0.225 kip.

The frame elements were assigned linear elastic properties and the transition meshes inelastic properties. The frame elements were assigned the gross moment of inertia and the gross area of the uncracked section of the double-tee beam. Because the middle, heated double-tee beam was connected to the transition meshes through node-to-node nonlinear springs, these meshes had to provide the same pattern of nodes so that each node in the double-tee beam had a corresponding node on the transition mesh at the same level to connect with. Therefore the transition mesh had the same mesh configuration and element type as the mesh of the middle double-tee beam. The frame elements were connected to the transition meshes by imposing a kinematic coupling constraint between the end node of the frame element, which is the reference node, and the nodes located on the surface of the transition mesh elements. This presupposes that the surface between the constrained nodes on the transition meshes remained plane, consistent with beam theory.

The same connection case was used across the span of the entire system in each case except at the node connecting each two adjacent frame elements in the five double-tee beam system, where full connectivity was provided. For instance, in the flange-only restraint case, the middle double-tee beam was connected to the adjacent transition meshes at each end through the flange-only connection, and the transition meshes at the far ends were connected to the ground through the flange-only connection as well.

The models were analyzed for each connection case and for each fire duration. **Table 3** shows the forces in the springs between the transition mesh and the double-tee beam on one side for the three double-tee beam system, and **Table 4** shows the forces for the five double-tee beam system. The direction of restraint moment was consistent with restraint condition. The flange-restraint case experi-

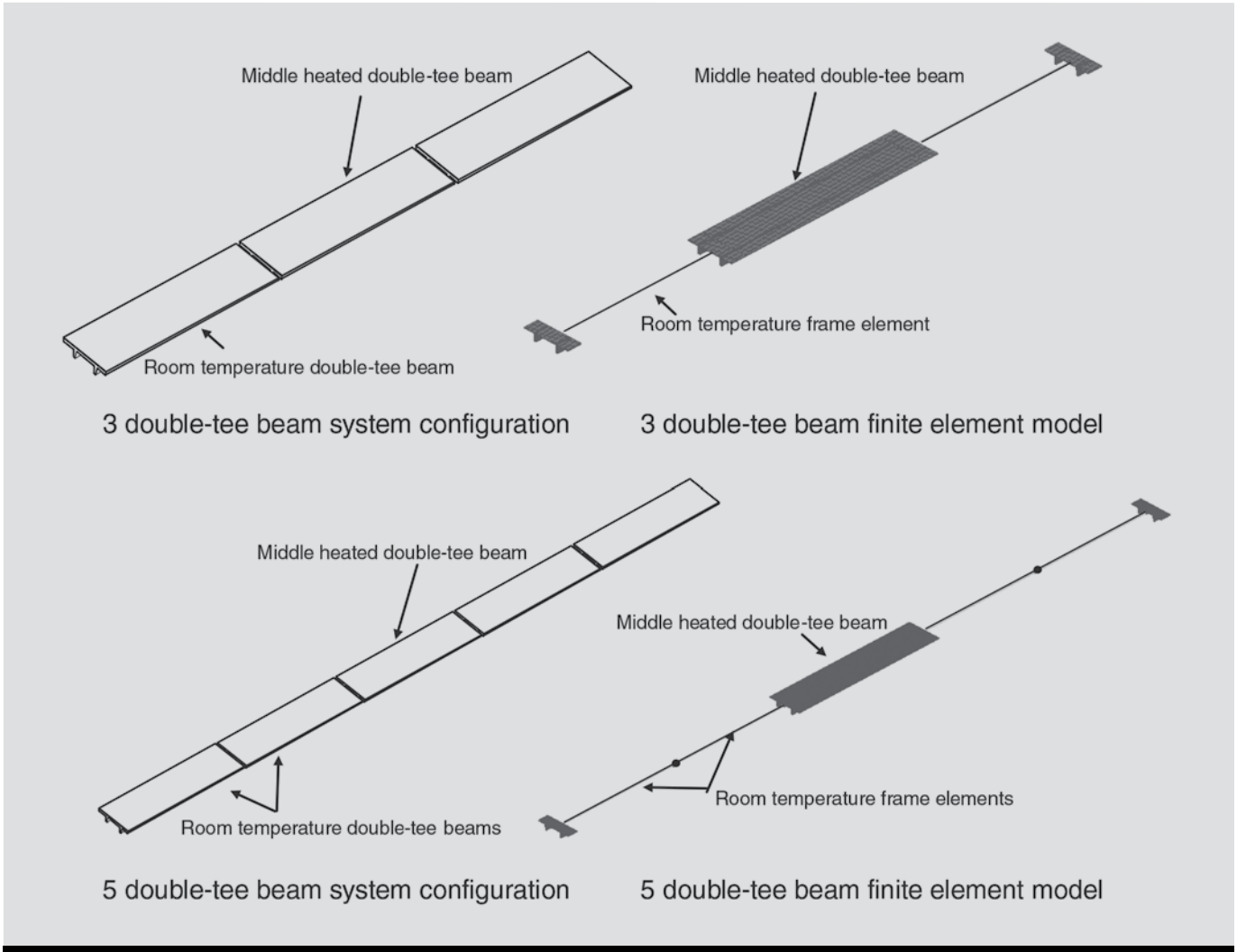

Figure 10. Double-tee beam systems and finite element models.

enced positive restraint moments throughout the duration of the fire, while the web-restraint case experienced negative restraint moments. The full-restraint case, however, experienced negative restraint moment during the early stages of the fire; the moment reversed in the three double-tee beam system but not in the five double-tee beam system. The reverse in moment direction in the three double-tee beam system took place at 2.0 hours and at 1.5 hours in the single-span idealized boundary condition. The magnitudes of the restraint forces in the five double-tee beam system were less than the corresponding values of the restraint forces in the three double-tee beam system. The restraint forces in both cases were less than the corresponding restraint forces in the idealized single-span cases. This shows that the restraint forces in a structural member tend to decrease as the flexibility of the system increases. The lower flexibility

Table 3. Restraint forces results for the 3 double-tee beam system

Load effect	Axial force, kN*				Bending moment, kN-m†			
Fire duration, hours	0.5	1.0	1.5	2.0	0.5	1.0	1.5	2.0
Full restraint	3935	5966	7270	7898	-326	-212	-67	77
Flange restraint	2618	4130	5225	5876	290	493	642	721
Web restraint	3582	5310	6390	6886	-409	-356	-247	-121

* Positive values are in compression.
† Positive value moments cause compression above neutral axis.
Note: 1 m = 3.28 ft; 1 kN = 0.225 kip.

Table 4. Restraint forces results for the 5 double-tee beam system

Load effect	Axial force, kN*				Bending moment, kN-m†			
Fire duration, hours	0.5	1.0	1.5	2.0	0.5	1.0	1.5	2.0
Full restraint	2556	4142	5404	6217	-146	-274	-167	-36
Flange restraint	1770	2945	3939	4649	196	343	479	566
Web restraint	2397	3826	4917	5587	-380	-366	-292	-181

* Positive values are in compression.
† Positive value moments cause compression above neutral axis.
Note: 1 m = 3.28 ft; 1 kN = 0.225 kip.

in the five double-tee beam system compared with the three double-tee system is attributed to the lower axial stiffness in the former due to its greater length. The stresses developed in the frame element were checked to ensure that the use of linear elastic properties for those elements is appropriate. These stresses are found to be less than 0.45 f'_c, the limit of the linear elastic behavior of concrete according to the American Concrete Institute's *Building Code Requirements for Structural Concrete (ACI 318-05) and Commentary (ACI 318R-05)*.[10] Therefore, assigning linear elastic properties to the frame elements is justified.

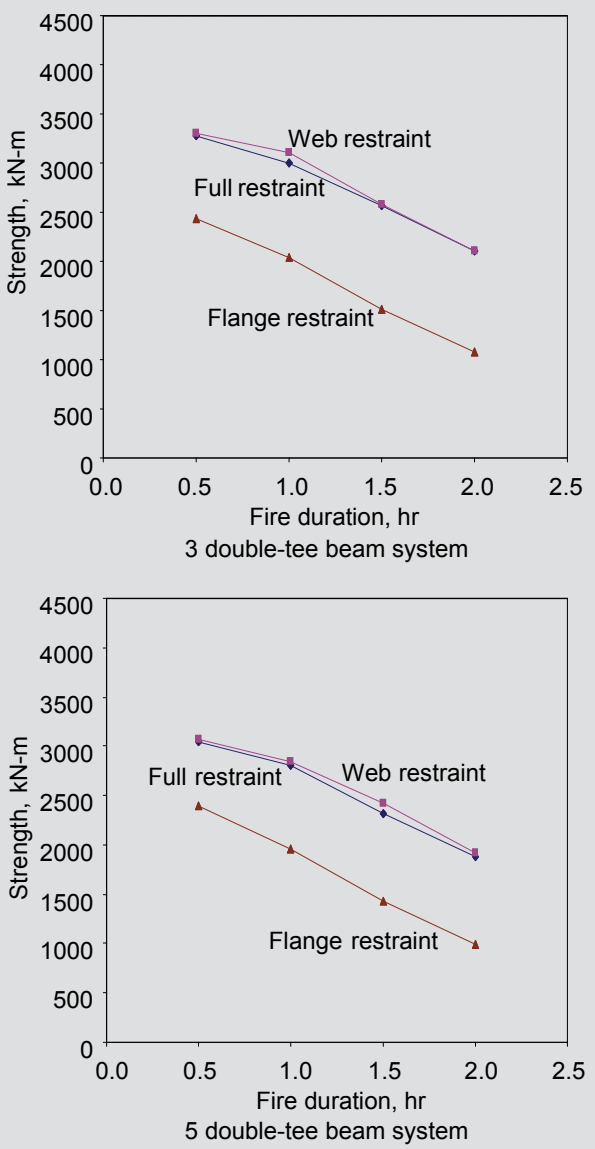

Figure 11. Summary of the strength analyses results for 3 double-tee beam system and 5 double-tee beam system. Note: 1 m = 3.28 ft; 1 kN = 0.225 kip.

Strength analyses

The same fiber models that have been explained and used in the idealized case were used here after replacing the previous restraint forces with those in Tables 3 and 4. **Figure 11** summarizes the results of the strength analyses of this case. For both the three and five double-tee beam systems at any given fire duration, the strength of the double-tee beam was slightly less with the full-restraint boundary conditions than with the web-restraint boundary conditions. This is because in the full-restraint case the flange contributes to the restraint, reducing the strength of the double tee. The strength is significantly less in the flange-only restraint case than the other two cases. By comparing these results with the self-weight midspan moment of one simply supported double-tee beam (that is, 778 kN-m [574 kip-ft]), the double-tee beam is expected to withstand its self-weight in all restraint cases and at all fire durations.

Figure 12 compares the results of the double-tee beam systems of the multiple-span restraint analyses and the results of the idealized restraints applied to the single-span beam. The strength of the double-tee beam decreased as the number of spans increased in all restraint conditions.

Spandrel beams and inverted-tee girders restraint

In precast concrete structural systems, the double-tee beams are often supported by spandrel beams and inverted-tee girders. The axial restraint to the double tee is provided in these cases by the weak-axis bending stiffness of the

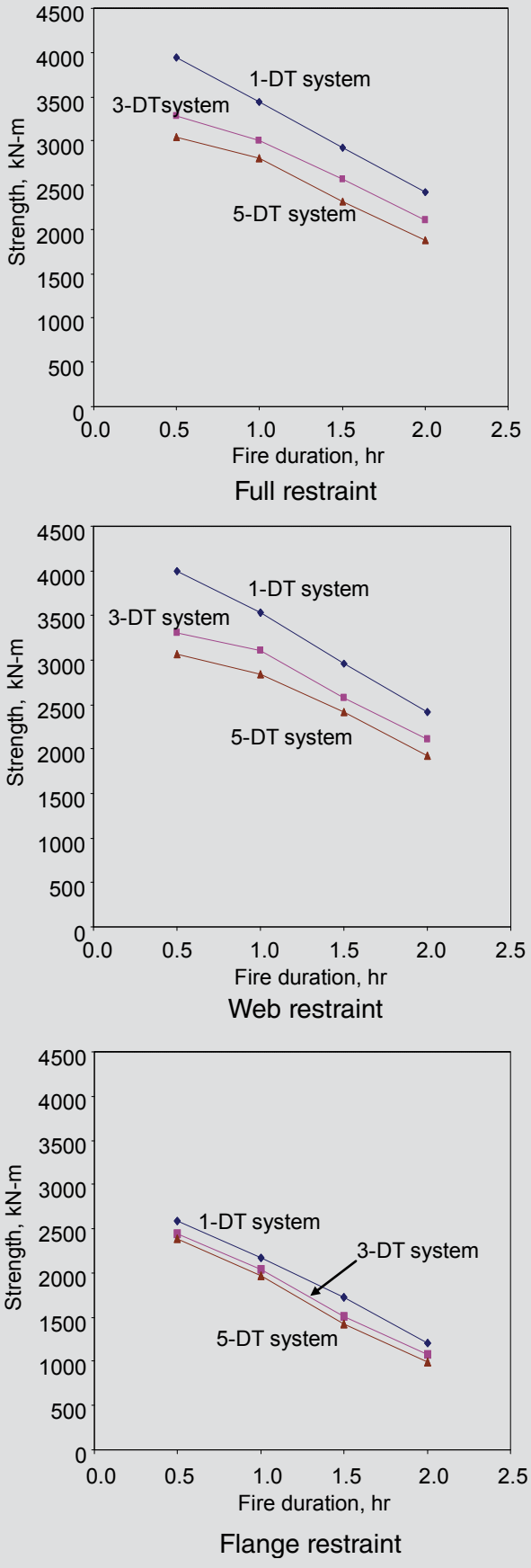

Figure 12. Comparison of the strength analyses results for varying the number of spans. Note: DT = double-tee. 1 m = 3.28 ft; 1 kN = 0.225 kip.

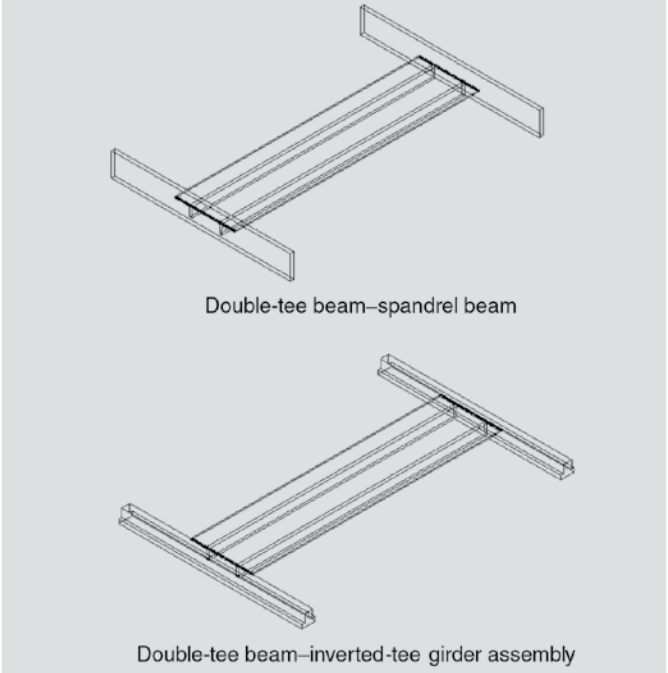

Figure 13. Assembly models.

spandrel beam or the inverted-tee girder. Typically, three double-tee beams are supported by one side of a spandrel beam or an inverted-tee girder. As an example of flexible supports, a pocket spandrel beam and an inverted-tee girder were considered in this paper and the behavior of a single double-tee beam supported by the spandrel beam or the inverted-tee girder was studied. The double-tee beam was positioned at midspan of the supporting element. The spandrel had a width of 280 mm (11 in.) and an overall depth of 1.8 m (72 in.). The inverted-tee girder had a web depth of 610 mm (24 in.), flange width of 1016 mm (40 in.), flange thickness of 292 mm (11.5 in.), and overall depth of 902 mm (35.5 in.). The effect of fire on the restraint provided by spandrel and the inverted tee and accordingly on the strength of the double-tee beam was evaluated.

Restraint forces analysis

Figure 13 shows the models of the double-tee beam–spandrel beam assembly and double-tee beam–inverted-tee girders assembly. The spandrel beam and the inverted-tee girder each had a span of 45 ft (13.7 m).

The double-tee beam had the same geometry, mesh, element type, and material properties used in the previous analyses. In addition, only the double-tee beam was exposed to the standard fire from underneath. The spandrel beam and inverted-tee girder remained at room temperature and retained their room temperature properties throughout the analyses. The compressive strength of the concrete in the spandrel beam was 34.8 MPa (5050 psi), and the compressive strength of the concrete in the inverted-tee girder was 69.5 MPa (10,080 psi).

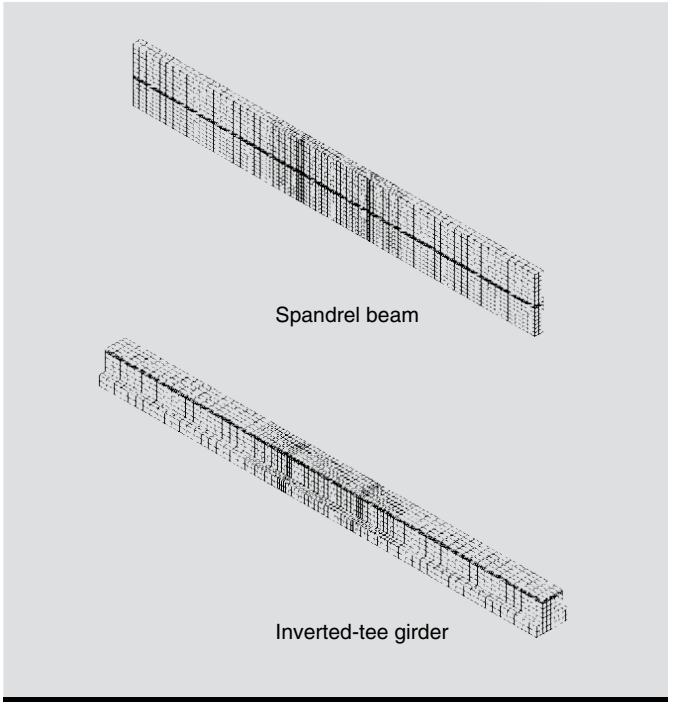

Figure 14. Mesh models.

The spandrel beam and inverted-tee girder were assigned linear elastic material properties to reduce the execution time of the analyses. The applicability of linear elastic properties was checked by studying the development of stresses in the models. The stresses generated in the inverted-tee girders and spandrels from the analyses added to the stresses from the self-weight, and the prestressing forces were found to be less than the linear elastic limits. However, they exceeded the tensile strength of the concrete at several locations. Had concrete cracking been included in the model, the resulting restraint forces would have decreased. Because neglecting the cracking in concrete results in an underestimate of the restraint forces, and because the exaggeration in the values of the restraint forces is found to be moderate (as will be shown later), assigning the linear elastic undamaged concrete properties was acceptable in these restraint force analyses.

The double-tee beam was connected from its flange to the web of the spandrel beam and inverted-tee girder through nonlinear compression-only springs. These springs were connected between each node on the flange of the double-tee beam at its end section and a corresponding node on the web of the spandrel beam or the inverted-tee girder. The meshes, therefore, of the spandrel beam and the inverted-tee girder were designed specifically to provide the nodes required to connect with the corresponding nodes on the double-tee beam by the nonlinear springs. Thus, the meshes of the spandrel beam and inverted-tee girder were compatible with the mesh of the flange of the double-tee beam in the region in contact with the double-tee beam flange section. The mesh became coarser outside that region to reduce the execution time of the analysis (**Fig. 14**).

The inverted-tee girders and spandrel beams were prescribed boundary conditions so that they behaved in a simply supported manner. These boundary conditions were intended to represent the manner in which the spandrel or inverted tee are connected to the supporting column.

Table 5 presents the restraint forces that were extracted from the structural analyses. The restraint forces and moments were less in the spandrel beam case than in the inverted-tee girder case. This is attributed to the fact that the spandrel beam had lower bending stiffness than the inverted-tee girder. The moments in the table are all positive because the restraint is flange restraint, which is consistent with the earlier observations.

Strength analyses

The same fiber models used in the previous analyses were used here after replacing the previous restraint forces with the ones in Table 5. **Figure 15** shows the results of the strength analyses and compares these results with those of the idealized single-span restraint cases. The behavior of the double-tee beam in both the spandrel beam restraint case and the inverted-tee girder restraint case was similar. Also, compared with the results of the idealized single-span restraints, the behavior of the double-tee beam in both the spandrel beam restraint case and the inverted-tee girder restraint case was similar to the behavior of the simply supported case. The increase in strength due to the flexible support elements was negligible.

Table 5. Restraint forces results for the flexible support elements cases

Load effect	Axial force, kN*				Bending moment, kN-m†			
Fire duration, hours	0.5	1.0	1.5	2.0	0.5	1.0	1.5	2.0
Spandrel beam	15	28	42	57	2	3	5	6
Inverted-tee girder	192	340	497	660	24	42	65	88

* Positive values are in compression.
† Positive value moments cause compression above neutral axis.
Note: 1 m = 3.28 ft; 1 kN = 0.225 kip.

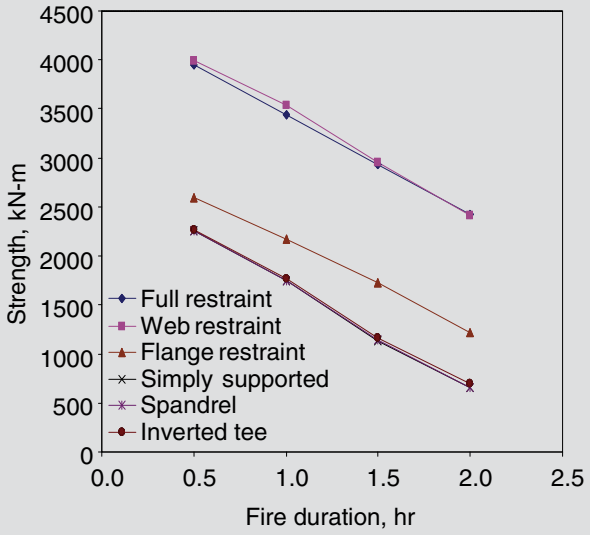

Figure 15. Strength analyses results for the flexible support elements cases compared with the idealized single-span cases. Note: 1 m = 3.28 ft; 1 kN = 0.225 kip.

Flange connectors

It is common practice in many precast concrete building systems to use regularly spaced flange connectors to join adjacent double-tee beams. Flange connectors compensate for varying camber, align the flanges in the out-of-plane direction, and resist many types of diaphragm forces. Flange connectors also transfer shear between panels. A precast, prestressed double-tee beam restrained along its span by flange connectors was analyzed. The same double-tee beam from the previous analyses was joined to an adjacent double-tee beam on each side by flange connectors (**Fig. 16**). The middle double-tee beam was exposed to standard fire from underneath. Analyses were performed to explore the significance of using different numbers of flange connectors on the restraint forces and the strength of the double-tee beam. Four different cases were considered,

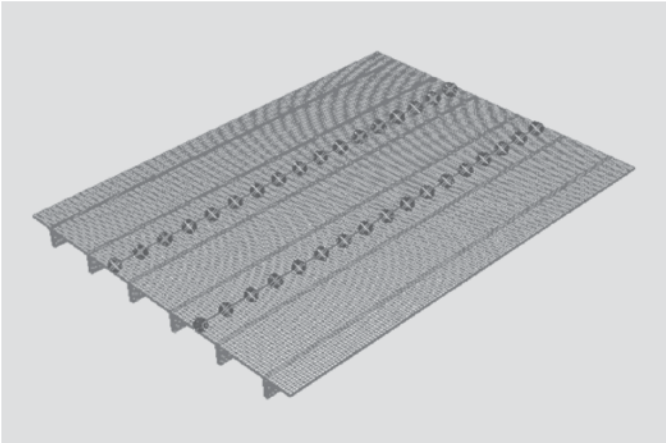

Figure 16. Finite element model for the 17 flange connectors case.

where the number of flange connectors varied along the span: 3, 5, 9, and 17 flange connectors. Seventeen flange connectors is an unrealistically large number from a practical point of view but was included to provide a high-end estimate of the restraint force that may develop.

Restraint forces analyses

Many types of connectors are used by the precast concrete industry. Although their purpose is basically the same, their individual behaviors differ. Oliva et al.[11] described the load deformation characteristics of flange connectors under horizontal shear, tension, and combined loading. These properties were used in this study. The vertical shear properties used were those of the V-connectors that were tested by Shaikh and Feile.[12] Each flange connector was modeled in the finite element analysis by three nonlinear springs. Each spring acted in a fixed direction parallel to one of the global Cartesian coordinate axes. The three directions simulated the behavior of the actual connectors in tension, horizontal shear, and vertical shear.

The middle double-tee beam had the same geometry, mesh, element type, and nonlinear material properties that

Table 6. Restraint forces results for the nonlinear connectors case

Load effect	Axial force, kN*				Bending moment, kN-m†			
Fire duration, hours	0.5	1.0	1.5	2.0	0.5	1.0	1.5	2.0
3 connectors	142	142	142	142	25	25	25	25
5 connectors	285	285	285	285	51	51	51	51
9 connectors	550	569	569	569	98	102	102	102
17 connectors	996	1112	1139	1139	178	198	203	203

* Positive values are in compression.

† Positive value moments cause compression above neutral axis.

Note: 1 m = 3.28 ft; 1 kN = 0.225 kip.

Table 7. Restraint forces results for the linear connectors case

Load effect	Axial force, kN*				Bending moment, kN-m†			
Fire duration, hours	0.5	1.0	1.5	2.0	0.5	1.0	1.5	2.0
3 connectors	469	921	1239	1577	89	164	231	282
5 connectors	690	1312	1899	2390	123	234	339	426
9 connectors	996	1871	2671	3330	178	334	478	594
17 connectors	1439	2626	3670	4475	257	469	655	799

* Positive values are in compression.
† Positive value moments cause compression above neutral axis.
Note: 1 m = 3.28 ft; 1 kN = 0.225 kip.

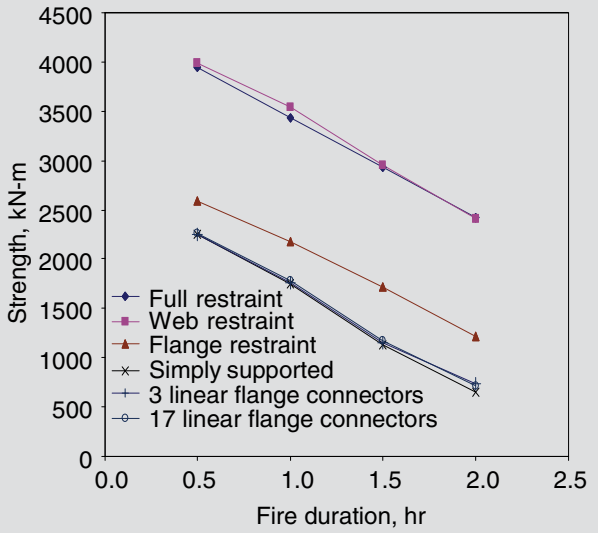

Figure 17. Strength analyses results for the linear flange connectors cases compared with the idealized single-span cases. Note: 1 m = 3.28 ft; 1 kN = 0.225 kip.

were discussed and used previously. In addition, only that double-tee beam was exposed to the standard fire from below to isolate the restraint provided by the connectors. The two adjacent double-tee beams remained at room temperature and retained their room-temperature properties. They, however, had the same geometry, mesh, and element type as the middle double-tee beam. Figure 16 shows the entire model of the 17 flange connectors case as an example of the other models considered. The boundary conditions prescribed to the models provided complete freedom of expansion to the three double-tee beams. Therefore, minimum restraints were prescribed only to prevent rigid body motion and matrix singularities.

Table 6 presents the restraint forces resulting from the analyses using nonlinear flange connectors. These restraint forces show that the flange connectors yielded at an early stage of the fire. Thus, the restraint forces in most cases were constant in the four fire durations considered. When compared with those from any of the previous analyses, the restraint forces in Table 6 are small. Their effect on the strength was found to be insignificant. By changing the connector properties with those of stronger connectors, the restraint forces are expected to increase accordingly. As an extreme case, the analyses were repeated using linear elastic properties in the three directions. The effect of using flange connectors with unlimited strength was used. The stiffnesses of the connectors prescribed in this case were the same as the initial stiffnesses used in the previous nonlinear connectors.

Table 7 presents the restraint forces resulting from the analyses using linear elastic flange connectors. As expected, the restraint forces in this case were significantly larger than those in the nonlinear case. In addition, in both the linear and nonlinear flange connectors' cases, the restraint forces developing in the double-tee beam increased with the increase in the number of flange connectors. The largest restraint forces developed in the case of the 17 linear flange connectors. These restraint forces were lower, however, than the restraint forces developed in the idealized flange-restraint case, which were the least among the other idealized cases.

Strength analyses

Strength analyses were conducted for only the cases of 3 and 17 flange connectors because the restraint forces developing in the other two cases lie between them. **Figure 17** shows the results of the strength analyses and compares them with those of the idealized single-span restraint cases. The strength of the double-tee beam restrained by 3 flange connectors was similar to that when restrained by 17 flange connectors. Thus, varying the number of flange connectors along the span of the double-tee beam had minimal influence on the strength added to the double-tee

beam during fires. In addition, the strength of the double-tee beam restrained by any number of flange connectors was similar to that of the simply supported double-tee beam. Therefore, flange connectors do not contribute to the restraint of double-tee beams during fires.

Conclusion

From the idealized single-span restraints analyses, the strength of the double-tee beam was found to vary significantly with the boundary conditions and when subjected to different durations of standard fire. The strength was significantly less in the flange-restraint case and even less in the simply supported case than in the web-restraint case and the full-restraint case. The strength of the double-tee beam in the web-restraint case was slightly higher than in the full-restraint case. This is attributed to the fact that the flange contributes to the restraint in the full-restraint case (which tends to decrease the strength) and does not in the web-restraint case.

From the multiple-span restraints analyses, in both the three and five double-tee beam systems, the strength of the beam in the web-restraint case was slightly higher than that of the full-restraint case and was considerably higher in both cases than in the flange-restraint case. This was consistent with the findings of the idealized single-span restraint analyses. In addition, the strength of the double-tee beam decreased as the number of spans increased in all restraint conditions. This effect, however, was lower in the flange-restraint case than in the other restraint cases.

From the flexible support elements (spandrel beams and inverted-tee girders) restraints analyses, the strength of the double-tee beam restrained by the flexible support elements was only slightly higher than the strength of the simply supported double-tee beam.

From the flange connectors restraints analyses, varying the number of flange connectors along the span of the double-tee beam had insignificant influence on the restraint mechanisms and the additional strength added to the double-tee beam during fires. Using flange connectors of any type leads to the same additional strengths provided to the double-tee beam subjected to fire. The strength of the double-tee beam restrained by any type and any number of flange connectors was only slightly higher than the strength of the simply supported double-tee beam.

Acknowledgments

This paper is based on research supported by a Daniel P. Jenny Fellowship provided by the Precast/Prestressed Concrete Institute. Additional support was provided by High Concrete Structures Inc., Metromont Corp., and Tindall Corp. The second author received his financial support to pursue his master's degree from a scholarship grant provided by the Fulbright Foreign Student Program, which is sponsored by the U.S. Department of State Bureau of Educational and Cultural Affairs. The sources of support noted here are gratefully acknowledged. The views expressed in this paper are those of the authors.

References

1. Gustaferro, A. H., and L. D. Martin. 1989. *Design for Fire Resistance of Precast Prestressed Concrete*. MNL-124-89. 2nd ed. Chicago, IL: PCI.

2. Okasha, N. M. 2007. "Analytical Evaluation of Restraint Mechanisms in Precast Concrete Double Tee Floor Systems Subjected to Fire Loading." MS thesis, Department of Civil and Environmental Engineering, Lehigh University, Bethlehem, PA.

3. Okasha, N. M., and S. Pessiki. 2006. "Analytical Evaluation of Restraint Mechanisms in Precast Concrete Double Tee Floor Systems Subjected to Fire Loading." ATLSS report 06-24, Lehigh University, Bethlehem, PA.

4. ASTM (American Society for Testing and Materials) E119. 2005. *Standard Test Methods for Fire Tests of Building Construction and Materials*. West Conshohocken, PA: ASTM.

5. ISO 834-2. 2009. *Fire-Resistance Tests—Elements of Building Construction Part 2: Guidance on Measuring Uniformity of Furnace Exposure on Test Samples.* Geneva, Switzerland: International Organization for Standardization.

6. Lie, T. T. 1992. *Structural Fire Protection*. Manuals and Articles on Engineering Practice, no. 78. New York, NY: American Society of Civil Engineers.

7. Eurocode 2 ENV 1992-1-2. 1996. "Part 1.2, General Rules-Structural Fire Design." In *Design of Concrete Structures*. Brussels, Belgium: European Committee for Standardization.

8. Thompson, J. M. 2004. "Behavior and Design of Precast Prestressed Concrete Inverted Tee Girders with Multiple Web Openings for Service Systems." PhD diss., Department of Civil and Environmental Engineering, Lehigh University, Bethlehem, PA.

9. PCI. 2004. *PCI Design Handbook: Precast and Prestressed Concrete*. MNL-120. 6th ed. Chicago, IL: PCI.

10. ACI (American Concrete Institute) 318. 2005. *Building Code Requirements for Structural Concrete (ACI 318-05) and Commentary (ACI 318R-05)*. Farmington Hills, MI: ACI.

11. Oliva, M. G., J. A. Pincheira, and F. I. Kusumo-Richard. 1998. Test on Double Tee Beam Flange Connectors Subjected to Monotonic and Cyclic Loading. *PCI Journal* 43 (3): 82–96.

12. Shaikh, A. F., and E. P. Feile. 2002. "Testing of JVI Vector Connector." University of Wisconsin-Milwaukee, WI.

Notation

C = specific heat (J/m^3°C)

f_c = compressive strength of concrete at temperature T

f_c' = cylinder strength of concrete at temperature T

f_{co}' = cylinder strength of concrete at temperature 20°C (68°F)

f_{pe} = effective stress of prestressing steel

f_{pu} = ultimate stress of prestressing steel

k = thermal conductivity (W/mºC)

T = temperature (ºC)

α = coefficient of thermal expansion of concrete

ρ_c = density of concrete (24,000 N/m^3)

About the authors

Nader Okasha received his PhD from the Department of Civil and Environmental Engineering at Lehigh University in Bethlehem, Pa. He is an assistant professor in the Department of Civil Engineering at the University of Hail in Hail, Saudi Arabia.

Stephen Pessiki is a professor of structural engineering in the Department of Civil and Environmental Engineering at Lehigh University in Bethlehem, Pa.

Abstract

This paper examines restraint mechanisms in precast, prestressed concrete structures under fire loading. The focus of the study is a prototype precast, prestressed double-tee beam typically used for precast concrete parking structures. The study examines idealized (simple and fixed) single-span restraints and three realistic restraint mechanisms:

- multiple-span successive spans
- gravity support elements (for example, spandrels or inverted-tee girders)
- flange connectors

The analytical approach included nonlinear heat transfer analysis of temperatures throughout a double tee at different fire durations and nonlinear structural analyses of restraint forces and flexural strengths. The strengths were found to vary significantly with boundary condition and fire duration. The strength is significantly less when only the flange is restrained compared with when only the web is restrained and when the entire cross section is restrained. The flexural strength of a beam restrained by spandrels or inverted-tee girders is only slightly greater than that of a simply supported beam. Finally, the strength of a beam restrained by any practical number of flange connectors is only slightly higher than that of a simply supported double-tee beam.

Keywords

Double tee, finite element analysis, fire, restraint, strength.

Review policy

This paper was reviewed in accordance with the Precast/Prestressed Concrete Institute's peer-review process.

Reader comments

Please address and reader comments to journal@pci.org or Precast/Prestressed Concrete Institute, c/o *PCI Journal*, 200 W. Adams St., Suite 2100, Chicago, IL 60606.